Journal of Crystal Growth 475 (2017) 44–48

Contents lists available at ScienceDirect

Journal of Crystal Growth

journal homepage: www.elsevier.com/locate/crys

Growth of $YbFe_2O_4$ single crystals exhibiting long-range charge order via the optical floating zone method

H.L. Williamson [a,*], T. Mueller [a], M. Angst [a], G. Balakrishnan [b]

[a] Jülich Centre for Neutron Science JCNS and Peter Grünberg Institut PGI, JARA-FIT, Forschungszentrum Jülich GmbH, 52425 Jülich, Germany
[b] Department of Physics, University of Warwick, Coventry CV4 7AL, UK

ARTICLE INFO

Article history:
Received 2 February 2017
Received in revised form 29 May 2017
Accepted 30 May 2017
Available online 1 June 2017
Communicated by T.F. Kuech

Keywords:
A1. X-ray diffraction
A1. Charge ordering
A2. Floating zone technique
B. $YbFe_2O_4$
B. $LuFe_2O_4$
B1. Rare earth compounds

ABSTRACT

We report the growth of $YbFe_2O_4$ single crystals via the floating zone technique, in four different oxygen partial pressures ranging from $CO:CO_2$ = 1:5 to 1:2.5, for a cross comparison of stoichiometry effects. We obtained highly stoichiometric single crystals with sharp magnetic transitions as well as off-stoichiometric samples with smeared transitions. We also provide for the first time clear evidence of 3D long-range charge order correlations at room temperature in $YbFe_2O_4$ through high energy X-ray diffraction, identical to the analogous $LuFe_2O_4$. The correlation length obtained for $YbFe_2O_4$ in the $\vec{c}$ direction is at least a factor of 5 larger than that observed in $LuFe_2O_4$.

1. Introduction

Magnetoelectric multiferroic materials are of great interest due to their potential integration into novel storage devices [1]. A particular focus has been placed on the RFe_2O_4 series (R = Lu, Yb, Y, Er, Ho and Tm) which crystallizes in the $R\bar{3}m$ space group [2], due to the once proclaimed ferroelectricity due to charge order (CO) between the Fe^{2+} and Fe^{3+} rich bilayers in $LuFe_2O_4$ [3]. However, recent findings suggest the Fe-O layers are themselves charged rather than polar, providing no ferroelectric state [4]. This system is both spin and charge frustrated, where the strong Ising nature of the system promotes both ferrimagnetic (fM) and antiferromagnetic (AFM) orders. The relative ion sizes of the rare earth elements in this series of compounds produce changes in both the cell volume and more profoundly the layer separation within an iron bilayer [5]. The difference in layer separation will have a strong effect on both the charge and spin order (SO), due to the intra- and interlayer interaction. This is seen clearly for example, in YFe_2O_4, which alters the magnetic properties and the CO configuration [6–9]. Based on the similar ion size of Lu^{3+} and Yb^{3+}, the magnetic properties, as well as the CO superstructure should lie in close relation to each other. Varying the oxygen stoichiometry through synthesis plays a large role in understanding the different characteristics of oxygen rich and deficient RFe_2O_4 samples, [5,6,10–16]. Particular focus has now been placed on $YbFe_2O_4$, the neighboring rare earth compound to the well studied $LuFe_2O_4$ [3,4,11,14–23], where currently few investigations reside [5]. A good indicator for viewing crystal quality in $LuFe_2O_4$ is the magnetization, whereas the few studies on $YbFe_2O_4$ exhibit an array of varying magnetization curves [10,24–31] similar to off-stoichiometric $LuFe_2O_4$ [17,25]. CO superstructure modulations in both $LuFe_2O_4$ and $YbFe_2O_4$ occur along (n/3, n/3, L) (n = integer), where the previous studies on $YbFe_2O_4$ exhibit only 2D diffuse CO seen in both Tunneling Electon Microscopy (TEM) studies [32] and more recently in synchrotron X-ray diffraction [33]. In both YFe_2O_4 and $LuFe_2O_4$ this low dimensionality in magnetism and CO was linked closely to oxygen deficiencies [5], indicating that synthesis conditions are still not optimal for the production of long-range order in $YbFe_2O_4$. The latest synchrotron data by [33] speculates strongly that $YbFe_2O_4$ exhibits only low dimensional CO, described as an incommensurate Charge Density Wave (CSW), which cannot be ferroelectric based on the incommensurately modulated dipole moments. However, in $LuFe_2O_4$ both 3D long-range order [4,15,20] and 2D short-range CO [21,34] is observed, the latter in off-stoichiometric samples. It is therefore imperative to see if by tuning the oxygen partial pressure environment through powder synthesis and crystal growth of $YbFe_2O_4$, 3D long-range CO could be achieved as in the case of $LuFe_2O_4$.

* Corresponding author.
E-mail address: h.williamson@fz-juelich.de (H.L. Williamson).

http://dx.doi.org/10.1016/j.jcrysgro.2017.05.034
0022-0248/

This paper describes extensive experimentation with different $CO:CO_2$ gas ratios, during single crystal growth via the traveling molten zone technique, leading to the production of highly stoichiometric single crystals. Powder X-ray diffraction and macroscopic magnetization measurements provide a basis for comparison for off-stoichiometry and crystal quality. Lastly, we show single crystal X-ray diffraction data highlighting for the first time 3D long-range CO in highly stoichiometric $YbFe_2O_4$.

2. Experimental procedure

Commercial powders of Yb_2O_3 (Alfa Aeser 99.9%) and Fe_2O_3 (Alfa Aeser 99.99%) were used as starting materials. Stoichiometric quantities were ground together thoroughly in an agate mortar and heated to 1200° C [35]. All stoichiometric powder mixtures were heated in a $CO:CO_2$ = 1:3 gas flow, based on previous successful synthesis and single crystal growth of isostructural $LuFe_2O_4$, using gas ratios between $CO:CO_2$ = 1:5 and 1:2.5 [16,20,36]. The stoichiometric powder was heated for 72 h at this temperature with intermediate grindings to promote homogeneity. The resulting powder was ground and isostatically pressed to produce polycrystalline rods of 6–8 mm in diameter and 60–70 mm in length. The rods were then sintered for 12 h in the same $CO:CO_2$ = 1:3 gas flow. Crystal growth was carried out by the floating zone method using a Crystal Systems Inc. F-ZT-10000-H-IV-VPS four mirror furnace. All crystals were grown at a speed of 1 mm/h and average rotation speed of 25/25 rpm for the feed and seed shaft, respectively. The individual gas ratios used for the crystal growths were $CO:CO_2$ = 1:5, 1:3.5, 1:3 and 1:2.5, where the typical pressure used during each crystal growth was set in the range of 1.25–1.75 bar. In some cases to promote homogeneity of melting for the main crystal growth, an initial fast scan (10 mm/h) was performed, which passes the molten zone through the entire polycrystalline rod. A small section of the crystal boule was cut out and ground for powder X-ray diffraction using a Huber Guinier D670, for phase purity analysis. Crystals ranging from 3 to 28 mg were obtained for magnetization measurements performed on a Cryogenic Inc. CCMS high field measurement system with VSM option, a Quantum Design Physical Properties Measurement System (PPMS) Dynacool and a Quantum Design Magnetic Properties Measurement System (MPMS). In-house single crystal X-ray diffraction was measured using a Rigaku Oxford diffraction SuperNova diffractometer with Mo-K_α. High energy X-ray diffraction was performed at the Advanced Photon Source (APS) on the beamline 6-ID-D.

3. Results and discussion

3.1. Powder diffraction

The $CO:CO_2$ = 1:5 atmosphere was first selected and used for crystal growth, based on a previous successful growth of a stoichiometric $LuFe_2O_4$ single crystal in this atmosphere [16]. The resultant crystal boule was about 5 cm in length and 5–6 mm in diameter, shown in Fig. 1 (top). The rod was a dull silver colour with multiple small lines running up its length. A small section of the rod was cut and the colour inside was light brown and powdery in texture. Powder X-ray diffraction indicated multiple phases including; Yb_2O_3, Fe_2O_3, $YbFe_2O_4$, $Yb_2Fe_3O_7$ and $Yb_3Fe_5O_{12}$. These phases are seen clearly in the phase diagram of Fe-Fe_2O_3-Yb_2O_3 [35], indicating a too high oxygen partial pressure. Further growths in lower oxygen partial pressure atmospheres yielded single phase $YbFe_2O_4$, e.g the crystal grown in $CO:CO_2$ = 1:2.5 shown in Fig. 1 (top). The growths with lower oxygen partial pressure were much more stable than that of the $CO:CO_2$ = 1:5, where only minor adjustments in input power were required for stability.

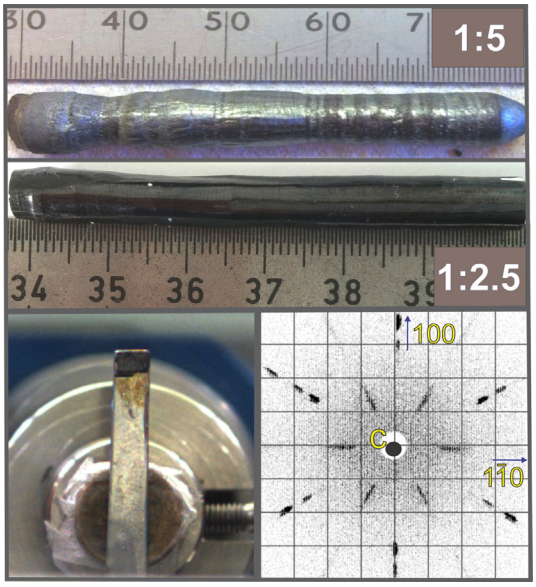

Fig. 1. Top: Crystals grown via optical floating zone in different oxygen partial pressures; $CO:CO_2$=1:5 and CO:CO = 1:2.5. Bottom: image of $YbFe_2O_4$ single crystal mounted on real time Laue camera (left), Laue image along c-direction (right).

Single crystals of $YbFe_2O_4$ show a strong tendency to cleave along facets perpendicular to the $\vec{c}$ direction, which is similar to the behaviour in $LuFe_2O_4$ [14,15]. Fig. 1 (bottom left) shows a stoichiometric single crystal (with M(T) comparable to Fig. 3 SC (inset)) mounted on a real time Laue set-up with dimensions $3 \times 2 \times 1$ mm, where the flat shiny facet is perpendicular to the $\vec{c}$ direction. The Laue image shown in Fig. 1 (bottom right) taken of a stoichiometric single crystal is perpendicular to $\vec{c}$.

Powder diffraction on four different samples are shown in Fig. 2. All samples grown in oxygen partial pressures between $CO:CO_2$ = 1:3.5 and 1:2.5 yielded single phase $YbFe_2O_4$ [37], indicating that under these conditions $YbFe_2O_4$ is stable. A Le Bail fit of both powdered single crystals (see Fig. 3 for magnetization curves performed on the two single crystals) grown in $CO:CO_2$ = 1:2.5 gave lattice parameters; a = 3.4578(3), c = 25.1285(9) and a = 3.4604 (3), c = 25.1320(5), with final refinement values of Rp = 1.51 and 1.58, respectively. There is only a small variation in lattice parameters, which we can consider not to be statistically significant. The difference between the powdered crystals, PSC and PNSC is discussed in Section 3.2.

3.2. Magnetization Studies

Our magnetization studies on field cooling (FC) from 300 to 10 K on three $YbFe_2O_4$ single crystals grown in $CO:CO_2$ = 1:2.5 Sample 1 (S1), 1:3 (S2) and 1:3.5 (S3) are shown in Fig. 3, with masses m = 32 mg, 4.5 mg and 3.5 mg, respectively. The crystals S2 and S3 grown in the more oxidizing conditions, the $CO:CO_2$ = 1:3.5 and 1:3, only exhibit smeared features and shifts in transition temperatures (Table 1) compared to the sharp features visible in S1 grown in the $CO:CO_2$ = 1:2.5 atmosphere. However sample to sample dependence occurs even in one crystal growth.

A clear example of this is shown in Fig. 3 (inset), which shows a comparison of magnetization curves from two crystals SC and NSC taken from the same growth in the $CO:CO_2$ = 1:2.5 atmosphere. The magnetization curve of SC is very similar to that of the S1 sample (black curve main panel), indicating a stoichiometry close to optimal, whereas the magnetization curve of NSC resembles more the S2 and S3 curves (red and blue curves in main panel, respectively).

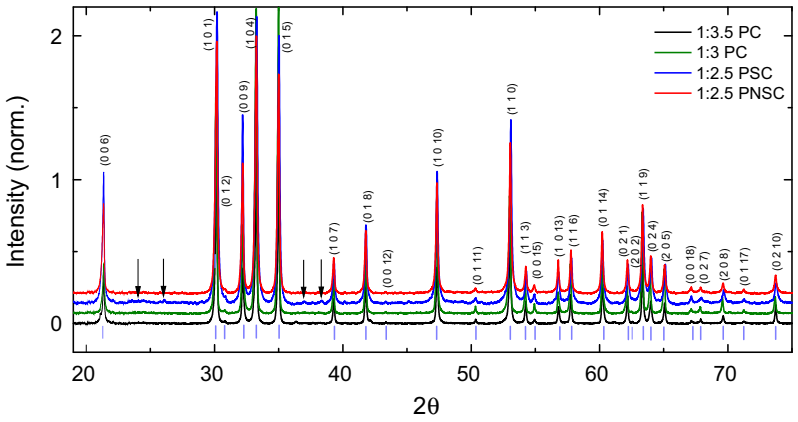

Fig. 2. Powder diffraction of $YbFe_2O_4$ on: 1:3.5 Powdered Crystal (PC), 1:3 (PC), 1:2.5 Powdered Stoichiometric single Crystal (PSC) and 1:2.5 Powdered Non-Stoichiometric single Crystal (PNSC) with background subtracted. Arrows indicate peaks from mylar foil used for the powder diffraction measurement, which occurs strongly in the (PSC) due to the smaller mass of powder obtained from the 20.8 mg, more stoichiometric single crystal. The reflection positions of the R$\bar{3}$m structure were taken from [37].

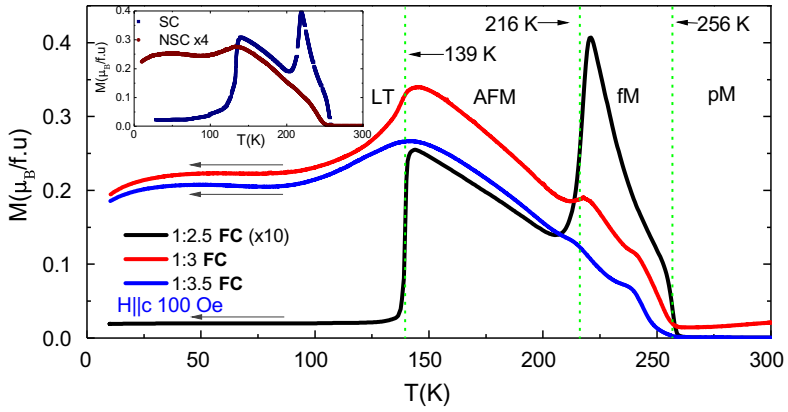

Fig. 3. Field cooled magnetization measured on three different single crystals grown in three $CO:CO_2$ gas ratios: $CO:CO_2$ = 1:2.5 Sample 1 (S1) (black curve), $CO:CO_2$ = 1:3 (S2) (red curve) and $CO:CO_2$-1:3.5 (S3) (blue curve). **Inset**: FC magnetization on a Stoichiometric single Crystal (SC) (blue curve), and Non-Stoichiometric single Crystal (Brown curve) scaled by x4, both grown in $CO:CO_2$ = 1:2.5, and later ground for powder diffraction and named PSC and PNSC, respectively. (For interpretation of the references to colour in this figure legend, the reader is referred to the web version of this article.)

Table 1
CO and magnetic properties overview of 5 different samples S1 to S5 grown in the 4 different atmospheres. The S1 to S3 samples all have relative magnetization measurements, where the CO in S1 was also investigated with X-ray diffraction at the APS. The three different magnetic transitions seen in each of these samples is stated as well as the width of the transition ΔT, which clearly indicates the broadness of the transitions. S4, a microgram size crystal, was measured solely on the in-house single crystal diffractometer to look at the type of CO present, also shown in Fig. 5 (top). Lastly, the S5 sample was taken for powder diffraction and found to be purely mixed phase, due to the higher oxygen partial pressure used during growth. The majority of crystals obtained from the growth in the $CO:CO_2$ = 1:2.5 exhibit 3D long-range CO. The appearance of long-range CO in crystals is greatly reduced with the use of higher oxygen partial pressures during growth.

Sample	Gas Ratio $CO:CO_2$	Single Phase	Magnetic transitions						Type of CO
			T_c	ΔT_c	T_{AFM}	ΔT_{AFM}	T_{LT}	ΔT_{LT}	
S1	1:2.5	Yes	256 K	8 K	216 K	16 K	139 K	8 K	3D
S2	1:3	Yes	249 K	18 K	214 K	8 K	113 K	58 K	–
S3	1:3.5	Yes	248 K	22 K	211 K	8 K	112 K	60 K	–
S4	1:3.5	Yes	–	–	–	–	–	–	2D
S5	1:5	Mixed Phase	–	–	–	–	–	–	–

These sample to sample dependences even within one crystal growth are however completely analogous to findings in both $LuFe_2O_4$ [14,15] and YFe_2O_4 [6], which also exhibit large sensitivity to oxygen stoichiometry.

Temperature dependent magnetization measurements on the well studied $LuFe_2O_4$, became a common tool for determining the sample quality [14,20], where single crystals grown in either a too reducing or too oxidizing gas ratio exhibited broad transitions [5,11,14–17,24]. The effect of off-stoichiometry in this series are not limited to $LuFe_2O_4$ and $YbFe_2O_4$, but large variations in the magnetic characteristics are also seen in YFe_2O_4 single crystals [6,9,38,39].

In order to obtain a better understanding of the different magnetic transitions present in $YbFe_2O_4$, a comparison can be made with the closely related $LuFe_2O_4$, based on the similar ion size of Lu^{3+} and Yb^{3+} [5]. Stoichiometric $LuFe_2O_4$ exhibits two transitions between room temperature (RT) and 10 K in low fields. The first, a Néel transition at T_N = 240 K to an apparently antiferromagnetic (AFM) phase, followed by a lower temperature glassy magnetic phase $\sim T_{LT}$ = 175 K [4,11,22,23,40,41] (Fig. 4 top). The

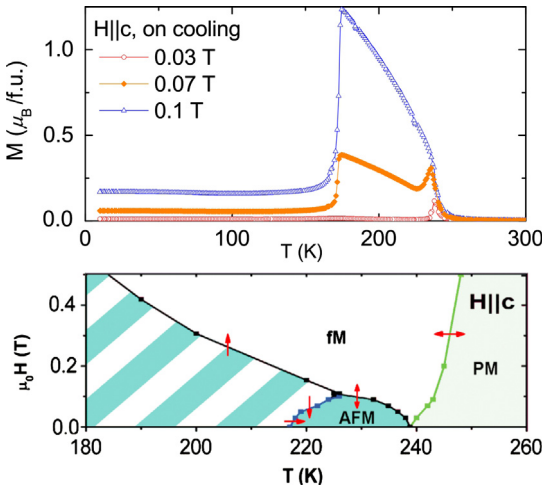

Fig. 4. $LuFe_2O_4$ for comparison, **Top**: Magnetization curves on field cooling, on a highly stoichiometric $LuFe_2O_4$ single crystal, measured with various externally applied fields. **Bottom**: H-T phase diagram exhibiting three magnetic phases; pM, AF and fM. Hatched area shows hysteretic region with competing fM and AF order, where either magnetic state can be stabilized. Arrows across phase lines indicate for which measurement direction it is observed given the hysteresis. (Taken from [14]) © 2012 American Physical Society.

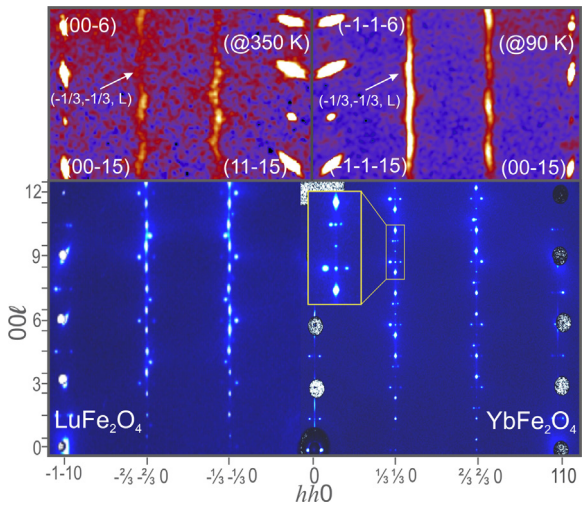

Fig. 5. Top: Reciprocal space precession images taken from the SuperNova single crystal diffractometer on a $YbFe_2O_4$ single crystal, grown in $CO:CO_2 = 1:3.5$. Left: 350 K and right: 90 K. **Bottom**: High energy X-ray diffraction of the HHL plane at 300 K. Left: A highly stoichiometric $LuFe_2O_4$ single crystal. Right: The highly stoichiometric $YbFe_2O_4$ (S1) single crystal grown in $CO:CO_2 = 1:2.5$. Structural reflections were covered with lead pieces to avoid over saturation and damage of the image plate.

magnetization measured in slightly higher fields revealed an additional fM phase that competes with the AFM phase, shown in Fig. 4 [14,15].

With particular focus on the most stoichiometric sample (S1) which can be readily understood in the context of the phases observed in $LuFe_2O_4$, the system goes into three different states at 100 Oe, on cooling. Phase 1; from RT to ~260 K the system is in a pM phase. Phase 2; resides between ~260 and 255 K, which goes from a pM phase to fM state, T_c. Phase 3; occurs on further cooling where the system goes from a fM to an AFM phase between ~220 and 210 K, T_{AFM}. Although, $LuFe_2O_4$ exhibits almost identical magnetic phases on cooling, the T_c transition in $YbFe_2O_4$ is shifted to a higher temperature of 256 K compared to $T_N = 240$ K in $LuFe_2O_4$. The onset of T_{LT} is much lower in $YbFe_2O_4$ at ~139 K, than 170 K seen in highly stoichiometric samples of $LuFe_2O_4$. A study of the magnetic structure of $YbFe_2O_4$ through neutron diffraction suggests that the spin structure in the different phases is very similar to that of $LuFe_2O_4$ [42].

3.3. Charge order studies

Single crystal X-ray diffraction on off-stoichiometric $YbFe_2O_4$ grown in $CO:CO_2 = 1:3.5$ is shown in Fig. 5 (top) and listed as S4 in Table 1. Reciprocal space precession images measured at 350 K (left) and 90 K (right), exhibit very similar 2D charge order (CO) modulations as seen in [33] which they describe intrinsically as a CDW. Crystals which exhibit this type of low dimensional CO modulation, produce magnetization curves similar to that shown in Fig. 3 (inset brown curve). The single crystals measured by Hearmon et al. [33] were grown in a $CO:CO_2 = 1:4$ gas ratio, from our powder diffraction and magnetization results this seems to be too oxidizing to produce long-range order.

High energy X-ray diffraction on the S1 crystal, which according to our magnetization studies is more stoichiometric (see Fig. 3 for M(T) (black curve)), was measured in the HHL plane at 300 K and is shown in Fig. 5 (bottom right). Clear, distinct Bragg spots are seen, quite different from the S4 sample with 2D diffuse scattering (Fig. 5 (top)). Highly stoichiometric $YbFe_2O_4$ exhibits an incommensurate CO pattern at room temperature, with correlations along (1/3, 1/3, L) and (2/3, 2/3, L), very similar to that of $LuFe_2O_4$ [4], shown in Fig. 5 (left). A single crystal refinement of this complex CO superstructure in $LuFe_2O_4$ was achieved [4]. The similarity of the CO seen in both the $LuFe_2O_4$ and $YbFe_2O_4$ can again be ascribed to the similar ion size of Lu^{3+} and Yb^{3+}, that in this case by tuning the oxygen partial pressure during crystal growth, 3D long-range CO is also established in $YbFe_2O_4$, where it is not intrinsically confined to short-range 2D correlations [33].

The long-range nature of the CO can be seen clearly in Fig. 6, where the peak widths of the Structural Reflection (SR) and nearest Super Structure Reflection (SSR) half integer peak are indistinguishable within resolution. The difference in the width of the SSR and SR peak, the latter of which gives an estimate of mosaicity and instrumental broadening, provides a finite correlation length [6]. Given the resolution we can estimate the minimum value of the correlation length in the $\vec{c}$ direction, which is ~40 nm. There are no current publications exhibiting long-range CO in $YbFe_2O_4$,

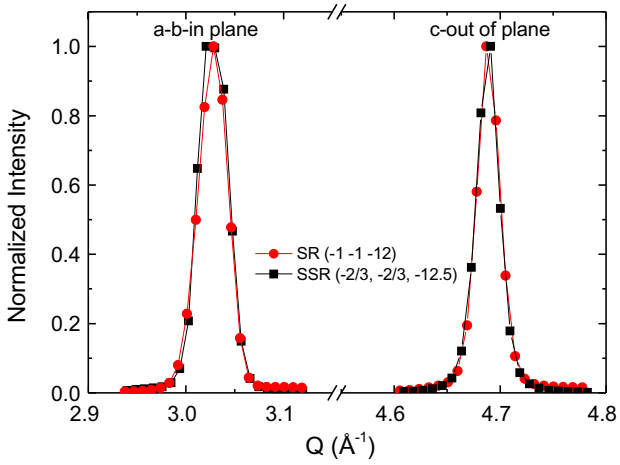

Fig. 6. Integrated intensity of: (-1-1-12) Structural Reflection (SR) (black curves) and Super Structure Reflection (SSR) (-2/3, −2/3, −12.5) (red curves) in plane and out of plane. X axis in reciprocal angstroms were converted from pixel, the displacement of peaks is due to pixels selected. (For interpretation of the references to colour in this figure legend, the reader is referred to the web version of this article.)

but a comparison can be made with correlation lengths obtained for $LuFe_2O_4$ from [40,43]. The correlation length calculated for the $\vec{c}$ directions by [40,43] was 7 nm and 6 nm, respectively. The correlation is therefore estimated to be at least a factor of 5 larger than $LuFe_2O_4$.

4. Conclusion and outlook

In summary we have grown highly stoichiometric single crystals of $YbFe_2O_4$, synthesized in the same image furnace used for the single crystal growth of stoichiometric $LuFe_2O_4$. The good stoichiometry is indicated by sharp magnetic transitions in macroscopic magnetization, the standard indicator for both $LuFe_2O_4$ and YFe_2O_4. It has allowed us to observe for the first time sharp charge order superstructure reflections, with correlation lengths at least a factor of 5 larger than those observed in highly stoichiometric $LuFe_2O_4$. Comparing qualitatively magnetization data and the CO superstructure pattern to those observed on sufficiently stoichiometric $LuFe_2O_4$, suggests that $YbFe_2O_4$ and $LuFe_2O_4$ are very similar in terms of both charge order and magnetism, which we attribute to the similar size of the rare earth elements. However, differences, for example in the relative stability of the ferrimagnetic phase were observed as well. The elucidation of such differences is the subject of ongoing work.

Acknowledgments

We gratefully acknowledge D. Robinson for the help with experimental set-up and data collection at the beamline 6-ID-D and P. Zakalek for the speedy creation of the 'peak finder' software, for analysis of the 6-ID-D imaging plate data. This research used resources of the Advanced Photon Source, a U.S. Department of Energy (DOE) Office of Science User Facility operated for the DOE Office of Science by Argonne National Laboratory under Contract No. DE-AC02-06CH11357. The 6-ID-D beamline was provided to the Advanced Photon Source by Forschungszentrum Jülich GmbH. Support from the initiative and networking fund of the Helmholz Association of German Research Centres by funding the Helmholz-University Young Investigators group "Complex Ordering Phenomena in Multifunctional Oxides" is gracefully acknowledged. Work at the University of Warwick was supported by EPSRC, UK, Grant EP/M028771/1).

References

[1] W. Eerenstein, N.D. Mathur, J.F. Scott, Multiferroic and magnetoelectric materials, Nature 442 (2006) 759–765.
[2] N. Kimizuka, A. Takenaka, Y. Sasada, T. Katsura, A series of new compounds $A^{3+}Fe_2O_4$A = Ho, Er, Tm, Yb, and Lu, Solid State Commun. 15 (1974) 1321–1323.
[3] N. Ikeda, H. Ohsumi, K. Ohwada, K. Ishii, T. Inami, K. Kakurai, Y. Murakami, K. Yoshii, S. Mori, Y. Horibe, H. Kito, Ferroelectricity from iron valence ordering in the charge-frustrated system $LuFe_2O_4$, Nature 436 (2005) 1136–1138.
[4] J. de Groot, T. Mueller, R.A. Rosenberg, D.J. Keavney, Z. Islam, J.W. Kim, M. Angst, Charge order in $LuFe_2O_4$: An unlikely route to ferroelectricity, Phys. Rev. Lett. 108 (2012) 187601.
[5] M. Angst, Ferroelectricity from iron valence ordering in rare earth ferrites?, Phys Status Solidi RRL 7 (2013) 383–400.
[6] T. Mueller, J. de Groot, J. Strempfer, M. Angst, Stoichiometric $YFe_2O_{4-\delta}$ single crystals grown by the optical floating zone method, J. Cryst. Growth 428 (2015) 40–45.
[7] N. Ikeda, R. Mori, K. Kohn, M. Mizumaki, T. Akao, Dielectric and structure properties of charge competing system YFe_2O_4, Ferroelectrics 272 (2002) 309–314.
[8] N. Ikeda, R. Mori, S. Mori, K. Kohn, Structure transition and charge competition on YFe_2O_4, Ferroelectrics 286 (2003) 175–184.
[9] J. Blasco, S. Lafuerza, J. García, G. Subías, V. Cuartero, J.L. García-Muñoz, C. Popescu, I. Peral, Characterization of competing distortions in YFe_2O_4, Phys. Rev. B 93 (2016), http://dx.doi.org/10.1103/physrevb.93.18411.
[10] M. Kishi, S. Miura, Y. Nakagawa, N. Kimizuka, I. Shindo, K. Siratori, Magnetization of $YbFe_2O_{4+x}$, J. Phys. Soc. Jpn. 51 (1982) 2801–2805.
[11] F. Wang, J. Kim, G.D. Gu, Y. Lee, S. Bae, Y.-J. Kim, Oxygen stoichiometry and magnetic properties of $LuFe_2O_{4+\delta}$, J. Appl. Phys. 113 (2013) 063909.
[12] H.X. Yang, H.F. Tian, Z. Wang, Y.B. Qin, C. Ma, J.Q. Li, Z.Y. Cheng, R. Yu, J. Zhu, Effect of oxygen stoichiometry in $LuFe_2O_{4+\delta}$ and its microstructure observed by aberration corrected transmission electron microscopy, J. Phys. Condens. Matter 24 (2012) 435901.
[13] K.T. Jacob, G. Rajitha, Nonstoichiometry, defects and thermodynamic properties of $YFeO_3$, YFe_2O_4 and $Y_3Fe_5O_{12}$, Solid State Ionics 224 (2012) 32–40.
[14] J. de Groot, K. Marty, M.D. Lumsden, A.D. Christianson, S.E. Nagler, S. Adiga, W. J.H. Borghols, K. Schmalzl, Z. Yamani, S.R. Bland, R. de Souza, U. Staub, W. Schweika, Y. Su, M. Angst, Competing ferri- and antiferromagnetic phases in geometrically frustrated $LuFe_2O_4$, Phys. Rev. Lett. 108 (2012) 037206.
[15] J. de Groot, Charge, spin and orbital order in the candidate multiferroic material $LuFe_2O_4$, Ph.D. thesis, RWTH Aachen, 2012.
[16] R.A. M[c] Kinnon, Studies of New Multiferroics, Master's thesis, University of Warwick, 2011.
[17] J. Iida, M. Tanaka, Y. Nakagawa, S. Funahashi, N. Kimizuka, S. Takekawa, Magnetization and spin correlation of 2-dimensional triangular antiferromagnet $LuFe_2O_4$, J. Phys. Soc. Jpn. 62 (1993) 1723–1735.
[18] Y. Yamada, S. Nohdo, N. Ikeda, Incommensurate charge ordering in charge-frustrated $LuFe_2O_4$ system, J. Phys. Soc. Jpn. 66 (1997) 3733–3736.
[19] Y. Yamada, K. Kitsuda, S. Nohdo, N. Ikeda, Charge and spin ordering process in the mixed-valence system $LuFe_2O_4$: Charge ordering, Phys. Rev. B 62 (2000) 12167–12174.
[20] A.D. Christianson, M.D. Lumsden, M. Angst, Z. Yamani, W. Tian, R. Jin, E.A. Payzant, S.E. Nagler, B.C. Sales, D. Mandrus, Three-dimensional magnetic correlations in multiferroic $LuFe_2O_4$, Phys. Rev. Lett. 100 (2008) 107601.
[21] Y. Zhang, H.X. Yang, Y.Q. Guo, C. Ma, H.F. Tian, J.L. Luo, J.Q. Li, Structure, charge ordering and physical properties of $LuFe_2O_4$, Phys. Rev. B 76 (2007) 184105.
[22] X.S. Xu, M. Angst, T.V. Brinzari, R.P. Hermann, J.L. Musfeldt, A.D. Christianson, D. Mandrus, B.C. Sales, S. McGill, J..W. Kim, Z. Islam, Charge order, dynamics, and magnetostructural transition in multiferroic $LuFe_2O_4$, Phys. Rev. Lett. 101 (2008) 227602.
[23] F. Wang, J. Kim, Y..J. Kim, G.D. Gu, Spin-glass behavior in $LuFe_2O_{4+\delta}$, Phys. Rev. B 80 (2009) 024419.
[24] J. Iida, Y. Nakagawa, N. Kimizuka, Field-heating effect - anomalous thermomagnetization curves observed in hexagonal $LuFe_2O_4$, J. Phys. Soc. Jpn. 55 (1986) 1434–1437.
[25] K. Yoshii, N. Ikeda, Y. Matsuo, Y. Horibe, S. Mori, Magnetic and dielectric properties of RFe_2O_4, $RFeMO_4$, and $RGaCuO_4$ (R=Yb and Lu, M=Co and Cu), Phys. Rev. B 76 (2007) 024423.
[26] C.R. Serrao, J.R. Sahu, K. Ramesha, C.N.R. Rao, Magnetoelectric effect in rare earth ferrites, $LnFe_2O_4$, J. Appl. Phys. 104 (2008) 016102.
[27] L. C-H, Y. Liu, F. Wang, X. Luo, S. Y-P, Z. X-Q, C. Z-H, Y. Sun, Photoinduced magnetization change in multiferroic $YbFe_2O_4$, Chin. Phys. Lett. 26 (2009) 127501.
[28] H.L. Williamson, Magnetic and Charge Order in $LuFe_2O_4$ and $YbFe_2O_4$ Multiferroics, noop Master's thesis, University of Warwick, 2012.
[29] K. Yoshii, N. Ikeda, Y. Nishihata, D. Maeda, R. Fukuyama, T. Nagata, J. Kano, T. Kambe, Y. Horibe, S. Mori, Exchange bias in multiferroic RFe_2O_4(R = Y, Er, Tm, Yb, Lu, and In), J. Phys. Soc. Jpn. 81 (2012) 033704.
[30] Y. Sun, Y. Liu, F. Ye, S. Chi, Y. Ren, T. Zou, F. Wang, L. Yan, A magnetoelectric multiglass state in multiferroic $YbFe_2O_4$, J. Appl. Phys. 111 (2012) 07D902.
[31] K. Fujiwara, M. Miyajima, M. Fukunaga, J. Kano, H. Kobayashi, N. Ikeda, Iron vacancy effect on the magnetization of $YbFe_2O_4$, Trans. Mater. Res. Soc. Jpn. 41 (2016) 139–142.
[32] Y. Murakami, N. Abe, T. Arima, D. Shindo, Charge-ordered domain structure in $YbFe_2O_4$ observed by energy-filtered transmission electron microscopy, Phys. Rev. B 76 (2007) 024109.
[33] A.J. Hearmon, D. Prabhakaran, H. Nowell, F. Fabrizi, M.J. Gutmann, P.G. R, Helical scattering signatures of strain and electronic textures in $YbFe_2O_4$ from three-dimensional reciprocal-space imaging, Phys. Rev. B 85 (2012) 014115.
[34] Y. Zhang, H.X. Yang, C. Ma, H.F. Tian, J.Q. Li, Charge-stripe order in the electronic ferroelectric $LuFe_2O_4$, Phys. Rev. Lett. 98 (2007) 247602.
[35] N. Kimizuka, T. Katsura, Standard free-energy of formation of $YbFe_2O_4$, $Yb_2Fe_3O_7$, $YbFeO_3$, and $Yb_3Fe_5O_{12}$ at 1200 ° c, J. Solid State Chem. 15 (1975) 151–157.
[36] J. Iida, S. Takekawa, N. Kimizuka, Single-crystal growth of $LuFe_2O_4$, $LuFeCoO_4$ and $YbFeMgO_4$ by the floating zone method, J. Cryst. Growth 102 (1990) 398–400.
[37] K. Kato, I. Kawada, N. Kimizuka, T. Katsura, Crystal-structure of $YbFe_2O_4$, Z Kristallogr 141 (1975) 314–320.
[38] T. Matsumoto, M. Nobuo, J. Iida, M. Tanaka, K. Siratori, Magnetic properties of the two dimensional antiferromagnets RFe_2O_4(R=Y, Er) at high pressure, J. Phys. Soc. Jpn. 61 (1992) 2916–2920.
[39] Y. Nakagawa, M. Inazumi, N. Kimizuka, K. Siratori, Low-temperature phase transitions and magnetic properties of YFe_2O_4, J. Phys. Soc. Jpn. 47 (1979) 1369–1370.
[40] J. Wen, G. Xu, G. Gu, S.M. Shapiro, Magnetic-field control of charge structures in the magnetically disordered phase of multiferroic $LuFe_2O_4$, Phys. Rev. B 80 (2009) 020403.
[41] M. Tanaka, K. Siratori, N. Kimizuka, Mössbauer study of RFe_2O_4, J. Phys. Soc. Jpn. 53 (1984) 760–772.
[42] H.L. Williamson, T. Mueller, G. Balakrishnan, M. Frontzek, M. Angst,}noop "unpublished"
[43] S. Park, Y. Horibe, Y.J. Choi, C.L. Zhang, S..W. Cheong, W. Wu, Pancake-like ising domains and charge-ordered superlattice domains in $LuFe_2O_4$", Phys. Rev. B 79 (2009) 180401.